Atmos. Chem. Phys. Discuss., 10, 821–862, 2010
www.atmos-chem-phys-discuss.net/10/821/2010/

Atmospheric Chemistry and Physics Discussions

This discussion paper is/has been under review for the journal Atmospheric Chemistry and Physics (ACP). Please refer to the corresponding final paper in ACP if available.

Anthropogenic aerosol radiative forcing in Asia derived from regional models with atmospheric and aerosol data assimilation

C. E. Chung[1], V. Ramanathan[2], G. Carmichael[3], S. Kulkarni[3], Y. Tang[3], B. Adhikary[3,*], L. R. Leung[4], and Y. Qian[4]

[1]Gwangju Institute of Science and Technology, Korea
[2]Scripps Institution of Oceanography, La Jolla, California, USA
[3]Department of Chemical & Biochemical Engineering, University of Iowa, Iowa City, USA
[4]Pacific Northwest National Laboratory, Washington, USA
[*]now at: School of Engineering, Kathmandu University, Dhulikel, Nepal

Received: 17 November 2009 – Accepted: 16 December 2009 – Published: 15 January 2010

Correspondence to: C. E. Chung (eddy@gist.ac.kr)

Published by Copernicus Publications on behalf of the European Geosciences Union.

Abstract

A high-resolution estimate of monthly 3-D aerosol solar heating rates and surface solar fluxes in Asia from 2001 to 2004 is described here. This product stems from an Asian aerosol assimilation project, in which a) the PNNL regional model bounded by the NCEP reanalyses was used to provide meteorology, b) MODIS and AERONET data were integrated for aerosol observations, c) the Iowa aerosol/chemistry model STEM-2K1 used the PNNL meteorology and assimilated aerosol observations, and d) 3-D ($X-Y-Z$) aerosol simulations from the STEM-2K1 were used in the Scripps Monte-Carlo Aerosol Cloud Radiation (MACR) model to produce total and anthropogenic aerosol direct solar forcing for average cloudy skies. The MACR model and STEM both used the PNNL model resolution of $0.45^{\circ} \times 0.4^{\circ}$ in the horizontal and of 23 layers in the troposphere.

The 2001–2004 averaged anthropogenic all-sky aerosol forcing is $-1.3\,\mathrm{W\,m^{-2}}$ (TOA), $+7.3\,\mathrm{W\,m^{-2}}$ (atmosphere) and $-8.6\,\mathrm{W\,m^{-2}}$ (surface) averaged in Asia (60–138° E and Eq. –45° N). In the absence of AERONET SSA assimilation, absorbing aerosol concentration (especially BC aerosol) is much smaller, giving $-2.3\,\mathrm{W\,m^{-2}}$ (TOA), $+4.5\,\mathrm{W\,m^{-2}}$ (atmosphere) and $-6.8\,\mathrm{W\,m^{-2}}$ (surface), averaged in Asia. In the vertical, monthly forcing is mainly concentrated below 600 hPa with maxima around 800 hPa. Seasonally, low-level forcing is far larger in dry season than in wet season in South Asia, whereas the wet season forcing exceeds the dry season forcing in East Asia. The anthropogenic forcing in the present study is similar to that in Chung et al. (2005) in overall magnitude but the former offers fine-scale features and simulated vertical profiles. The interannual variability of the computed anthropogenic forcing is significant and extremely large over major emission outflow areas. Given the interannual variability, the present study's estimate is within the implicated range of the 1999 INDOEX result. However, NCAR/CCSM3's anthropogenic aerosol forcing is much smaller than the present study's estimate at the surface, and is outside of what the INDOEX findings can support.

ACPD
10, 821–862, 2010

1 Introduction

Anthropogenic aerosols can modify climate directly by altering the radiative fluxes of the planet (Coakley and Cess, 1985; Charlson et al., 1991), and indirectly by altering cloud properties (Twomey, 1977; Albrecht, 1989; Rosenfeld, 2000). Aerosol radiative forcing is defined as the effect of aerosol, both natural and anthropogenic, on the radiative fluxes at the top of the atmosphere (TOA) and at the surface and on the absorption of solar (and long-wave in case of dust and sea salt particles) radiation within the atmosphere. The direct effect of aerosols on solar radiation, i.e., direct radiative forcing (DRF), has been estimated locally as well as globally in recent years.

A common procedure to estimate DRF is the use of simulated aerosol distributions as input to a radiative transfer model. Simulated aerosol masses are converted into aerosol optical properties by empirical/theoretical algorithms, and then converted into DRF by radiative transfer models. Kinne et al. (2003) summarized this procedure and also compared various aerosol simulations. As explained in Kinne et al. (2003), uncertainties in aerosol simulations arise from emission sources, meteorology and aerosol/chemistry processing. An independent approach is to use observations of aerosol optical properties such as aerosol optical depth (AOD) and single scattering albedo (SSA) to compute DRF. Aerosol observations are available from field campaigns, aerosol observation networks and satellite retrievals. Recent examples of this approach are Chung et al. (2005)[1] and Yu et al. (2006).

The present study integrates these two approaches by using simulated aerosols that are nudged towards aerosol observations. This "aerosol observation assimilation" has been conducted before (Collins et al., 2001), and retains advantages of both approaches. Aerosol simulations offer spatially ($X-Y-Z$) and temporally continuous values, while aerosol observations offer presumably better accuracy. In this study, we attempt to improve Collins et al. (2001) study by a) employing a high-resolution regional

[1]Chung et al. (2005) substituted aerosol simulations in areas where aerosol observations were not available.

ACPD
10, 821–862, 2010

climate model instead of a coarse-resolution global climate model and b) using ground and satellite aerosol observations. Giorgi et al. (2002) adopted a regional model to simulateaerosols but did not assimilate aerosol data.

In our study, the regional climate simulation is constrained by global reanalyses throughout the model domain to provide atmospheric forcings for a regional scale chemistry-aerosol model. In turn, the chemistry-aerosol model assimilates ground and satellite aerosol observations to simulate observationally constrained aerosols. The simulated aerosols are incorporated in a radiative transfer model to estimate aerosol radiative forcing. In Sects. 2 and 3 of this paper, we describe this procedure overall, and we describe the aerosol forcing in detail in Sect. 4. Adhikary et al. (2008) detail the aerosol simulation in a parallel study.

The regional domain for our study is Asia. Asia contains about 60% of the world's population with rapid economic and industrial growth. It contributes about 30 to 50% of the anthropogenic aerosol burden and is a major source of black carbon in the atmosphere. Regional scale modeling is necessary to capture the spatial heterogeneity associated with orography and emissions in Asia, and to better resolve atmospheric and aerosol processes.

2 The Asian aerosol assimilation project

The results in the present study are the products of a collaborative project between Scripps Institution of Oceanography (SIO), Pacific Northwest National Laboratory (PNNL), and the University of Iowa. As Fig. 1 illustrates, the PNNL regional climate model simulates meteorological variables that were used by the University of Iowa chemistry transport model STEM-2K1 (Sulfur Transport dEposition Model; version 2001) to simulate aerosols. The regional meteorological variables simulated by the PNNL model as well as the aerosol extinction coefficients simulated by the STEM-2K1 were then used in the SIO Monte-Carlo Aerosol Cloud Radiation (MACR) model to simulate anthropogenic aerosol radiative forcing.

2.1 PNNL regional climate model

The PNNL regional climate model is based on the Penn State/NCAR Mesoscale Model MM5 (Grell et al., 1995). The model has been used to simulate regional climate of the US (e.g., Leung et al., 2003; Gustafson and Leung, 2007) and East Asia (Leung et al., 2004; Qian and Leung, 2007), and found to generally well reproduce a wide range of climatic regimes in those regions. The model domain was expanded for this study. A major weakness, however, was found in simulating the interannual variations of the East Asian summer monsoon rainfall (Qian and Leung, 2007), which was related to model weaknesses in simulating the interannual variations of the large scale monsoon circulation in a large model domain. To ameliorate this problem, simple nudging was applied to constrain the large scale circulation of the regional model by a global reanalysis in this study. The interannual variability simulation improved.

The regional climate model was applied at 60 km horizontal grid resolution with 23 vertical levels for the domain shown in Fig. 2. The regional climate simulation was initialized on 1 September 1998 and ran through 31 December 2005. The physics parameterizations used in this study include the Kain-Fritsch cumulus convection scheme (Kain and Fritsch, 1993), the Reisner mixed phase cloud microphysics scheme (Reisner et al., 1998), the Community Climate Model (CCM3) shortwave and longwave radiation scheme (Kiehl et al., 1994), a nonlocal boundary layer transfer scheme (Hong and Pan, 1996), and the Noah land surface model (Chen and Dudhia, 2001).

The simulation was driven by lateral boundary conditions and SSTs from the NCEP/NCAR global reanalysis (Kistler et al., 2001) using a simple relaxation scheme that blends the global reanalysis and the model solution over a 15-grid point wide buffer zone in the lateral boundaries. To provide larger constrain on the large scale circulation, winds and temperature simulated by the model were continuously nudged towards the global reanalysis throughout the domain. A nudging coefficient of $5{\cdot}10^{-5}\,s^{-1}$ was used between the simulated planetary boundary layer and the model top. Over the oceans, the nudging coefficient increases from zero at the surface to $5{\cdot}10^{-5}\,s^{-1}$ at the

top of the boundary layer and remains constant above to allow nudging of winds and temperature throughout the atmospheric column.

Three hourly outputs for all the three-dimensional meteorological variables and two-dimensional surface variables were archived to provide atmospheric conditions for driving the STEM-2K1. Adkihary et al. (2007) used the same meteorological model outputs from this simulation for 2004–2005 to simulate aerosols over Asia. They evaluated the aerosol simulations against observations collected from the Atmospheric Brown Cloud-Post-Monsoon Experiment (ABC-APMEX) over two sites including the Kathmandu Observatory and the Hanimaadhoo Observatory in the Maldives. The regional climate model was found to provide realistic meteorological conditions for simulating aerosols over the two sites.

2.2 U. Iowa STEM

The Sulfur Transport dEposition Model (STEM-2K1) was used to generate the 3-D aerosol distributions from 2001 to 2004. The model version used in this study was developed in 2001 and hence the model name STEM-2K1 (hereafter referred to as STEM). The STEM has been extensively used previously to study aerosols and trace gases during this time period in South and Southeast Asia (Adhikary et al., 2007; Carmichael et al., 2003; Guttikunda et al., 2005; Tang et al., 2004). This is the first time that STEM has been used to simulate high resolution (both spatial and temporal) aerosol concentration over multiple years such that average annual aerosol distribution with intra/interannual variability can be analyzed.

The STEM for this study uses the PNNL regional model to drive the aerosol transport. The domain size and resolution of the STEM model are the same as those of the PNNL model as in Fig. 2. The STEM simulates BC (black carbon), OC (organic carbon), sulfate, dust and sea salt. Further details of the STEM parameters are discussed elsewhere (Adhikary et al., 2007). Here we present important highlights. Anthropogenic emission inventory used in this study is primarily from the emission inventory developed

for the 2001 NASA Transport and Chemical Evolution over the Pacific (TRACE-P) intensive field campaign (Streets et al., 2003). These emission estimates have been used extensively in Asian modeling studies and have been evaluated against data obtained in comprehensive field experiments (Huebert et al., 2003; Carmichael et al., 2003). Since this study domain is bigger than TRACE-P domain, emission data from EDGAR database were used to fill the extended geographical areas (Olivier and Berdowski, 2001). The anthropogenic emissions were held constant during the 4-year period, as only recently have the emission estimates for 2006 been produced (Zhang et al., 2009). The growth in SO_2 and BC emissions from 2001 to 2006 for Asia is estimated at ~35% and ~10%, respectively. Monthly varying emissions of carbonaceous aerosols from biomass burning are included in this study based on published emission datasets (var der Werf et al., 2006). The carbonaceous aerosol emission from biomass burning from 2001 to 2004 was used and interpolated from a $1^{\circ}\times1^{\circ}$ resolution. The emissions of sea salt are based on the parameterization of S. L. Gong (Gong, 2003). Dust emissions are calculated online based on the methodology discussed by Tang et al. (2004). The emissions of carbonaceous and sulfate aerosols are assumed to be in the sub-micron range (diameter < 1 µm). Sea salt emissions are calculated for fine mode (less than 2.5 µm) and coarse mode (2.5 µm<diameter<10 µm). Dust emissions are modeled using two size bins: sub-micron and super micron (1 µ*m*<diameter < 10 µm). Sulfate and sea salt aerosols are treated as a function of relative humidity while other aerosols are not.

2.3 SIO MACR model

3-D aerosol extinction coefficients simulated by the STEM were averaged monthly as an input for the Monte-Carlo Aerosol Cloud Radiation (MACR) model. The MACR model was originally developed and validated during the INDian Ocean EXperiment (INDOEX) (Satheesh et al., 1999; Podgorny et al., 2000; Podgorny and Ramanathan, 2001; Ramanathan et al., 2001) to compute solar fluxes and aerosol direct radiative

forcing (DRF). Chung et al. (2005) upgraded the model (see their study for the model details). For this study, we further upgraded the model by i) adjusting spatial domain and vertical coordinate and ii) modifying gas absorption coefficients.

To account for cloud influences on aerosol radiative forcing, we took climatological cloud data from ISCCP (International Satellite Cloud Climatology Project) D2 product (Rossow and Schiffer, 1999), as in Chung et al. (2005), and then modified them using the MODIS cloud fraction (MOD08_M3). In this data integration, we used a higher-resolution ($1^{\circ}\times1^{\circ}$) and year-to-year variations in MODIS overall cloud fraction, while retaining cloud separation into low, mid, high and deep convective, and cloud optical properties in ISCCP. Temperature and pressure fields were obtained from the PNNL regional model and monthly averaged for an input. The MACR model was run to produce monthly aerosol forcing from 2001 to 2004. The anthropogenic portion was calculated by removing sea salt and dust contributions in aerosol extinction coefficients. The STEM model provides aerosol extinction coefficient for each aerosol species. Though treating all the dust particles as natural is a crude approximation, the overall errors from such an assumption appear small compared to other assumptions and approximations in the present study. We plan to refine our calculation in the future.

3 Overview of aerosol data assimilation

In this study, the STEM aerosol simulation was nudged towards the observed aerosol data. The aerosol data assimilation method is described in detail in Adhikary et al. (2008). The current study improved the assimilation procedure slightly and a summary is given here.

Assimilated data are Daily Level 2 AOD products from MODIS (MODerate Imaging Spectro-radiometer) and Level 2 AODs from AERONET (AErosol RObotic NETwork). MODIS onboard the Terra satellite gives near-global coverage, while AERONET is a ground based observation network. Spatially continuous MODIS AODs and

sparsely-distributed AERONET AODs were integrated as in Chung et al. (2005), where the pattern of MODIS AODs was combined with AERONET AOD values. Chung et al. (2005) also give detailed information about AERONET and MODIS observations. MODIS retrieved products also include fine mode AODs and coarse mode AODs. This size separation was also used for the present study. The large uncertainty in aerosol related estimates of anthropogenic and natural emission estimates is one of the main motivations for constraining model-derived aerosol distributions with these observations. The MODIS and AERONET AODs reflect spatial and temporal (including inter-annual) variations in regional emissions (as well as transport and removal processes). Additionally, Kim and Ramanathan (2008) found that MODIS aerosol data are accurate enough as input for radiative flux simulation within instrumental errors.

MODIS and AERONET observations are assimilated with STEM aerosol calculation here using optimal interpolation technique initially developed for meteorological applications (Lorenc, 1986). The optimal interpolation methodology for assimilating satellite data has also been implemented in other chemical transport models such as ROSE (Research for Ozone in the Stratosphere and Its Evolution) and MOZART2 (Khattatov et al., 2000). We implemented the optimal interpolation technique similar to the methodology described by Collins et al. for INDOEX aerosols using their MATCH model (Collins et al., 2001). There are, however, some differences in our assimilation methodology, which are discussed later. First we present the mathematical relationship between the posterior aerosol distribution (analysis) with the model predicted aerosol (background) and satellite based observation (observation) in Eq. (1):

$$\tau'_{\mathrm{m}} = \tau_{\mathrm{m}} + \mathbf{K}(\tau_{\mathrm{o}} - \mathbf{H}\tau_{\mathrm{m}}) \,. \quad (1)$$

τ'_{m} is the posterior AOD while τ_{o}, and τ_{m}, are the observed and modeled AOD, respectively. **K** is the Kalman gain matrix and **H** is a linear interpolator from model space to observation space. Since we have transformed the observed AOD into the STEM model grid, the **H** matrix is simply the identity matrix. The **K** matrix is calculated based on the

ACPD
10, 821–862, 2010

background and observation error covariance matrices and is defined by Eq. (2):

$$\mathbf{K} = \mathbf{B}\mathbf{H}^T(\mathbf{H}\mathbf{B}\mathbf{H}^T + \mathbf{O})^{-1}. \quad (2)$$

Here **B** and **O** are the error covariance matrices of the background and the observation fields, respectively. Detailed discussion and assumption used to derive the **B** and **O** matrices are discussed by Collins et al. (2001). In Eqs. (3) and (4) we simply restate the mathematical relationship defining the **B** and **O** matrices and the values of the parameters that we have used in our assimilation process similar to the ones suggested for assimilating INDOEX aerosols.

$$\mathbf{O} = (f_o\tau_o + \varepsilon_o)^2 I \quad (3)$$

Here ε_o (equal to 0.04) is the minimum Root Mean Square (RMS) error of the observation and f_o (equal to 0.5) is the fractional error in observed AOD. *I* refers to identity matrix.

$$\mathbf{B}(d_x, d_y) = (f_m\tau_m + \varepsilon_m)^2 \exp\left[-\frac{d_x^2 + d_y^2}{2l_{xy}^2}\right] \quad (4)$$

Here ε_m is the minimum RMS uncertainty in the modeled AOD, which is set to 0.1 and f_m, the fractional error in the model AOD, is set to 0.5. Variables d_x and d_y are the horizontal distance between two model grid points (equal to 50 km) and l_{xy} is the horizontal correlation length scale for errors in the model fields which is set to 250 km (five grid cells).

The methodology for generating the assimilated aerosol distributions is as follows. First, STEM predicts three dimensional aerosol concentrations every three hours for all four years. This output is then averaged to produce monthly-mean three dimensional aerosol distributions. These distributions are then used to calculate AOD using chemical specie specific extinction coefficients. The extinction coefficient parameters used in STEM are reported in Penner et al. (2001). The STEM generated AODs are then used for assimilation of the AODs derived from MODIS observations, corrected

with AERONET AODs as mentioned earlier. Our methodology differs from Collins et al. (2001) in that we also assimilate sea salt aerosol while their work chose to keep the modeled sea salt distribution fixed. Another difference in our assimilation technique is that we utilize both the coarse mode (total minus fine mode) and fine mode AOD available from MODIS. In this methodology, if there is no fine mode fraction available for the model grid point, then the assimilation is done only using total AOD. We chose to adjust the anthropogenic aerosols, namely sulfate, black carbon and organic carbon using the observed fine mode AOD, while dust and sea salt are adjusted based on the assimilated coarse mode AOD. At each time step and model layer the mass mixing ratios of the aerosols are adjusted by the ratios of monthly assimilated AOD to monthly simulated AOD. Finally we used the available AERONET SSA data to adjust absorbing aerosols. The effect of nudging the aerosol simulation towards AERONET SSA will be further discussed later.

Figure 2 illustrates the overall assimilation procedure for March 2001. Monthly AODs from MODIS are shown in Fig. 2a. The MODIS AODs were corrected with AERONET AODs, referred to as "MODIS+AERONET AOD" for brevity here (Fig. 2b). Note that the number of AERONET sites in the domain changes from month to month from 4 to 22. The STEM simulated AODs before any aerosol data assimilation are displayed in Fig. 2c. After the assimilation, the final AODs are shown in Fig. 2d. The final AODs, which were used as input to the aerosol radiative forcing calculations as discussed next, appear similar to the MODIS+AERONET AODs where the latter are available. The STEM simulated AODs replaced the gaps for locations where MODIS+AERONET AOD values are missing. Our data assimilation technique is in a way a tool for transition from MODIS+AERONET AOD areas to their gaps. Even in areas where MODIS+AERONET AOD exists, our assimilation technique provides additional valuable information such as aerosol vertical profiles and composition needed to accurately compute aerosol radiative forcing.

The forward model (before assimilation) predictions of AOD show that the STEM model is able to capture many of the major features shown in the observed

distributions, including high values over the major emission sources and outflow regions. March is a high dust month and the STEM model for March 2001 shows high AOD over and downwind of the major dust source regions, including East Asia and the Middle East. The dust predictions for March and April of 2001 in East Asia have previously been discussed in detail, including comparison with observations of aerosol mass and composition obtained during the TRACE-P and ACE-Asia experiments (Tang et al., 2004), where the simulations were shown to be reasonably consistent with aircraft observations. After assimilation, the final AOD distribution closely matches the observation-based distributions.

In Fig. 3, the simulated and then nudged AODs in our study are compared to the GOCART (Georgiatech-Goddard Global Ozone Chemistry Aerosol Radiation and Transport) model (Chin et al., 2002) simulated AODs during March–May (MAM period). Our AODs produced with a higher resolution regional model and a formal assimilation procedure display more fine scale features than the GOCART AODs. In South Asia, aerosols trapped in the Indo-Gangetic valley are simulated in our study, and in East Asia, our simulated AODs are not stretched as far to Korea and Japan as are GOCART AODs. Figure 3 also displays MAM period AODs from Chung et al. (2005) used in a previous estimate of aerosol radiative forcing. Chung et al. (2005) AODs resemble aspects of both the present study calculations and GOCART simulations. In next section, we will discuss the difference with Chung et al. (2005) estimates in detail and their impact on estimated aerosol radiative forcing.

The four-year mean assimilated model distribution of AOD is shown in Fig. 4. Also shown are the anthropogenic AOD and BC AOD distributions, and the average PM_{10} surface mass concentration. The anthropogenic contribution from fossil and biofuel combustion dominates over most of Asia, with the largest impacts from dust and open burning found in the Middle East and the western China, and Southeast Asia, respectively. A distinguishing feature of Asia is a large contribution of BC to total AOD throughout much of Asia.

An evaluation of the STEM model skill in the forward mode in calculating AOD and aerosol mass concentrations and composition against a year long data set for 2005 available from the ABC project and an AERONET site in South Asia is presented in Adhikary et al. (2007). The model was shown to be able to capture the seasonal trends and magnitude of the observed AOD at both the Kanpur and Hanimaadhoo sites. This study also reported that the STEM modeled fine to coarse mode aerosol mass ratio agreed with the seasonal variation of observed angstrom exponent (an indicator of aerosol size) at Hanimaadhoo. An evaluation of the STEM assimilated distributions along with an analysis of their sensitivity to the optimal interpolation technique was presented in detail in Adhikary et al. (2008). In the present study, we have used the same optimal interpolation technique with minor modifications. Illustrative results are shown in Fig. 5, where computed AOD and surface PM_{10} are compared with observations. Observations in Fig. 5 are from AERONET AODs, MODIS AODs and EANET PM. The AERONET AODs obtained in 2005 were used as input for the aerosol data assimilation implemented in this study. Recently obtained AERONET AOD data have updated and expanded values, and this newer AERONET product is referred to as "AERONET new" in Fig. 5. We use "AERONET new" as an independent data set to evaluate the assimilation results.

As seen in Fig. 5, the assimilated AOD distributions are shown to capture the seasonal variability over a wide range of conditions from sites dominated by wind blown dust (Al Dhafra), to sites at island locations in the outflow from major continents (Male and Okinawa), to sites in major urban areas (Kanpur and Chulalongkorn). The computed surface PM_{10} is compared to available observations from the ABC project and the EANET (2004) monitoring network. The 4-year annual PM_{10} distribution is shown in Fig. 4, where high PM_{10} values are found throughout Asia as a result of wind blown dust, open burning and anthropogenic activities. The PM_{10} observations are rather limited during these years, however the model is able to capture regional differences and variability over a wide geographical area. Additional discussion of the aerosol composition and the component contributions to AOD in these computed fields

ACPD
10, 821–862, 2010

are available in Carmichael et al. (2009).

Of particular interest from a radiative forcing perspective is the estimation of BC distributions and AOD. A comparison of predicted surface BC mass concentrations at ABC sites has been presented and discussed in Adhikary et al. (2007), where the model was shown to accurately predict the BC observed at Hanimadhoo (seasonality and magnitude), and to underpredict peak values in Kathmandu. Recently BC estimates using global aerosol models have been compared with observations under the AeroCom project (Koch et al., 2009). In general, the BC mass and AOD predicted by these models for the Asia sub-domain were found to be biased low by a factor of two. Our assimilated field of BC AOD shown in Fig. 4, which takes into consideration AERONET SSA in the assimilation, compares well with the AERONET and OMI derived absorption AOD (AAOD) (see Fig. 3 in Koch et al., 2009). For example, the AAODs from AERONET are in the 0.02 to 0.03 range in the outflow regions around India and China, and above 0.05 in the Indo Ganges plain, and in the China megacity influenced regions around Beijing, Shanghai and the Pearl River Delta.

To further verify the simulated aerosol in this study beyond AOD, we examine BC (Black Carbon) concentration vertical structures in Fig. 6. BC vertical structure is an extremely important component of aerosol data in calculating anthropogenic aerosol radiative forcing and 3-D aerosol heating rate. From 6 March to 31 March 2006, Maldives Autonomous UAV (Unmanned Aerial Vehicle) Campaign (MAC Campaign) took place (Ramana et al., 2007; Corrigan et al., 2007; Ramanathan et al., 2007). The MAC yielded BC concentration vertical structures over 73.18° E and 6.78° N in most of March 2006, and we calculated the monthly mean. Figure 6 compares the BC data from the MAC with the present study calculation at a nearby grid. First, it is encouraging that the observed BC concentration magnitude is approximately in the simulation range. Second, the observed BC is maximum around 1500–2000 m height as a result of blending boundary layer aerosol structure data and lifted aerosol structure data. The simulated BC vertical profile at a nearby grid, however, tends to show boundary-layer structures. On the other hand, the simulated BC concentration near the surface is not

particularly stronger than the simulated concentrations above the boundary layer, and we find this feature an improvement. Textor et al. (2006) reported vertical profiles of simulated aerosols from various models (see Fig. 10 of Textor et al., 2006) where near-surface aerosol concentrations are far stronger than those above the boundary layer. Third, there is a large interannual variation of BC concentration at this location. More discussion on interannual variability follows in the next sections.

4 Anthropogenic aerosol forcing

The SIO MACR model was used to convert aerosol extinction coefficients into aerosol radiative forcing. The anthropogenic portion of the computed direct aerosol radiative forcing is shown in Fig. 7 and subsequent figures. In these figures, forcing estimates are for all skies and not for clear skies.

Figure 7 displays the 2001–2004 averaged forcing at the surface, in the atmosphere and at the top of the atmosphere (TOA). F(TOA), i.e., aerosol forcing at the TOA, is negative for the entire domain (Fig. 7a). Negative values are particularly pronounced in the Northern Indian Ocean. F(S) and F(A) have comparable magnitudes and opposite signs. As a result, F(S) and F(A) are much larger than F(TOA) in magnitude, since F(TOA)=F(S)+F(A). F(S) mirrors F(A) except over the Persian Gulf. F(S)/F(TOA) as in Fig. 7d shows the relative importance of atmospheric forcing. In South Asia and most coastal areas, F(S)/F(TOA) is noticeably big.

Chung et al. (2005) also estimated direct anthropogenic aerosol forcing by using MODIS+AERONET AODs and AERONET SSAs. Recently, Myhre (2009) evaluated global direct aerosol forcing estimates in IPCC Assessment Report IV and placed Chung et al. (2005) estimate at the best accuracy. The present study differs from Chung et al. (2005) in many respects. We use aerosol data assimilation to deal with data gaps and provide vertical structures while Chung et al. (2005) assumed uniform vertical aerosol profiles and used GOCART aerosol simulation to fill the gaps. Plus, this study employed high-resolution models. The result differences between the current study

and Chung et al. (2005) are summarized in Table 1. Averaged over Asia (60–138° E and Eq. −45° N), the present study finds the TOA forcing to be −1.3 W/m^2 in comparison with −1.1 W/m^2 from Chung et al. (2005). In the atmosphere, this study yields +7.3 W/m^2 while Chung et al. (2005) gives +8.0 W/m^2. We repeated the MACR model without the BC component in order to calculate the BC radiative forcing. We did this, given accelerating interests in the role of BC since Ramanathan and Carmichael (2008) reported the global direct BC TOA forcing to be +0.9 W/m^2 using Chung et al. (2005) calculations. Note that the global anthropogenic CO_2 forcing is only about 1.6 W/m^2 (IPCC Assessment Report IV; Ramanathan and Carmichael, 2008). Our current BC TOA forcing estimate in Asia is +2.1 W/m^2 when Chung et al. (2005) gives +2.3 W/m^2. Differences between these two estimates are overall very small.

The fact that the present study and Chung et al. (2005) give very similar estimates despite a number of different steps taken indicates that aerosol observation is the primary importance in calculating direct aerosol forcing. To be sure, we computed anthropogenic aerosol forcing without using AERONET SSAs also, and obtained surprisingly less BC concentration. As a result, the Asia-averaged anthropogenic aerosol forcing was −2.3 W/m^2 at TOA, +4.5 W/m^2 in the atmosphere and −6.8 W/m^2 at the surface without using AERONET SSAs. BC forcing was +1.2 W/m^2 at TOA, +4.4 W/m^2 in the atmosphere and −3.2 W/m^2 at the surface, compared with +2.1 W/m^2 at TOA, +7.3 W/m^2 in the atmosphere and −5.2 W/m^2 at the surface with AERONET SSAs in Table 1. This sensitivity test points to extreme importance in using aerosol absorption observations. The results with AERONET SSAs are what we consider more accurate and are reported in the figures. Figure 8 shows F(A) at 775 hPa in the months of January, April, July and October. F(A), i.e., aerosol forcing in the atmosphere, is another source of diabatic heating and is able to burn low-level clouds and/or disturb atmospheric circulation quickly. 775 hPa F(A) varies from almost zero to 1.0 K/day or more, and as such exhibits strong spatial gradients. Superimposed on F(A) in Fig. 8 are contours representing climatological precipitation derived by Xie and Arkin (1996). F(A) maxima tend to be located away from highly precipitating areas, but notable exceptions

include F(A) over the Indo-Gangetic valley in July. In spite of monsoon precipitation, aerosol concentration is large over there, because of week to two weeks long monsoon breaks (intervals between rain events).

Figure 9 displays the vertical structure of F(A) in South Asia in February. F(A) at 850 hPa and F(A) at 700 hPa appear similar with different magnitudes. Vertical cross sections at 76° E and at 20° N show most of the forcing between the surface and 600 hPa with maxima around 800 hPa. It is interesting to note that maximum aerosol heating rate is often located far above the surface when the simulated aerosol concentration is largest near the surface. To our belief, this is because absorbing aerosols above low-level clouds lead to larger solar heating rate than the same aerosols below clouds. Note that simulated aerosol concentration near the surface is only slightly larger than those between 800 and 900 hPa. If aerosol concentration is uniform vertically as assumed in Chung et al. (2005), aerosol solar heating rate would have conspicuous maximum values around 800 hPa. As seen from Fig. 6, observed aerosol concentration peaks above 1km over Maldives. This would lead to a very large aerosol solar heating rate above 1km. The importance of aerosol solar hearing rate vertical profile in affecting surface temperature and precipitation was examined by Chung and Zhang (2004) who demonstrated that climatic effects of absorbing aerosols are very sensitive to the vertical profile of aerosols. The vertical structure of F(A) in East Asia is quite similar to that in South Asia (Fig. 9).

Figures 11 and 12 demonstrate year-to-year variability of F(S) (aerosol forcing at the surface) in South Asia and East Asia. The interannual variability in F(S) is quite sizable, and very large in some areas. Averaged over 40–100° E and Eq. –20° N, January–March average of F(S) fluctuates from $-6.2\,W/m^2$ (2004) to $-14.7\,W/m^2$ (2002), giving the 4 year mean $-11.1\,W/m^2$ (Table 2). At a single grid point, interannual variability can be even greater, as seen in Fig. 6. Interannual variability is also large in East Asia (Fig. 10). The Yellow Sea and East Sea (i.e., Sea of Japan) areas show very large interannual variability but not the eastern Cina where there is a lot of industrial capacity. Similarly, over South Asia, large interannual variability occurs downstream.

ACPD
10, 821–862, 2010

Observations collected downstream should be collected for many years in order to give reliable climatological estimates.

The vertical profile of climatological atmospheric forcing for the dry season (January–March) is contrasted with that for the wet season (June–August) in Fig. 13. For South Asia, the forcing is largest between 1 km and 2 km from the surface. Observational studies with the UAV Campaign over the Maldives showed that aerosol solar heating reach peak values slightly above 2 km (Ramana et al., 2007; Corrigan et al., 2007), roughly consistent with our simulation. The dry season near-surface forcing is a factor of 3 larger than the wet season forcing in our estimate. In case of East Asia, seasonal variation is the opposite. The wet season forcing is larger. Strong seasonality in the South Asian heating seems largely due to seasonal variation in meteorological conditions since surface emission of aerosol precursors maintains similar values throughout a year. In East Asia, the wet season is associated with higher anthropogenic AODs, corresponding comparably to higher heating. This is due to anthropogenic aerosols soaring in summer every year. This period has the weakest flow and the strongest secondary aerosol production, both leading to extended periods between precipitation events with high aerosol loadings. These computation results need further corroboration from observation studies.

In Fig. 14, we compare our F(S) estimate with Chung et al. (2005) and the CCSM3 simulation for March–May (MAM) period. The CCSM3 (Community Climate System Model Version 3) (Collins et al., 2006) is the state-of-the-art NCAR (National Center for Atmospheric Research) coupled model. We ran the CCSM3 with and without BC, OC and sulfate aerosols, and took the difference. The CCSM3 was run in a mode in which observed SSTs and standard land surface output replaced the ocean and land surface model components. The F(S) estimates in our study and Chung et al. (2005) are much greater than the simulation by the CCSM3. Chung et al. (2005) estimate is overall similar to the estimate in the present study in magnitude. However, the present study offers much detailed features that can be useful as input for regional climate modeling. The annual mean F(S) shows similar relationship between the present study, Chung et

al. (2005) and the CCM3 simulation. Please note that our anthropogenic computation was obtained by taking the difference between the total-aerosol run and natural-aerosol run, just like in the CCSM3 experiment.

5 Summary and discussion

Here, we have sought to synthesize a collaborative study between Scripps Institution of Oceanography (SIO), Pacific Northwest National Laboratory (PNNL), and the University of Iowa. In our collaboration, i) the PNNL regional model bounded by the NCEP reanalyses provided meteorology in Asia, ii) SIO integrated MODIS and AERONET data for aerosol observations, iii) the Iowa aerosol/chemistry model STEM-2K1 used the PNNL meteorology to simulate aerosols and the STEM aerosol simulation was nudged towards aerosol observations, and iv) SIO converted the aerosol simulation into total and anthropogenic aerosol direct solar radiation forcing (DRF) for average cloudy skies. To our knowledge, the present study is the first attempt to employ a regional model in an aerosol data assimilation mode. This paper has also described the calculated anthropogenic aerosol radiative forcing (DRF).

The primary finding is that Asia-averaged anthropogenic forcing from the present study is similar to that from Chung et al. (2005) which also used MODIS and AERONET data. When AERONET SSAs were not used, our aerosol assimlation yielded much less BC concentration which led to much less warming forcing in the atmosphere and much less cooling forcing at the surface. Only with AERONET SSAs, is the present study able to match the computation in Chung et al. (2005). Since the present study employs high-resolution regional modeling, it offers fine-scale structures of aerosol forcing and simulated vertical profile – features not available in Chung et al. (2005). The accuracy of the global anthropogenic direct aerosol forcing estimate in Chung et al. (2005) was recognized by Myhre (2009).

Another progress in this study is the vertical structure of the calculated aerosol concentration and atmospheric aerosol forcing. As Textor et al. (2006) showed, aerosol

concentrations in typical aerosol simulation models are concentrated near the surface. Our simulated aerosols also have the largest concentration near the surface but have relatively uniform profiles from the surface to 700 hPa, in closer agreement with observation studies (Ramana et al., 2007; Corrigan et al., 2007; Ramanathan et al., 2007). The calculated anthropogenic aerosol forcing in the atmosphere is mostly between the surface and 600 hPa with maxima around 800 hPa. Our aerosol forcing has maxima above surface, due mainly to low-level cloud that amplifies aerosol forcing above it. Different vertical structures of forcing, though the vertical integrations might be the same, can give very different climate responses. Chung and Zhang (2004) demonstrated that the direct aerosol heating of near-surface air increases Convective Available Potential Energy (CAPE) whereas the heating above boundary layer decreases CAPE. Furthermore, absorbing aerosols located within low cloud can burn cloud condensate therein (so-called aerosol semi-direct effect; Ackerman et al., 2000), thereby increasing solar radiation reaching the surface. Near-surface concentrated aerosols in typical aerosol simulation models, if implemented into global climate models, would likely paint a misleading picture of the climatic effects of aerosols.

Although the anthropogenic aerosol forcing estimate in the present study is similar, in an Asia-averaged sense, to that of Chung et al. (2005), these two estimates are much greater than the simulated forcing by the CCSM3. How accurate is each estimate? The Indian Ocean Experiment (INDOEX) integrated comprehensive observations and led to aerosol forcing estimates over the South Asian area for 1999 (Ramanathan et al., 2001). We take the INDOEX results as a benchmark foraerosol forcing evaluation. In Table 2, we compare anthropogenic aerosol forcings obtained from the INDOEX, Chung et al. (2005), the present study and the CCSM3. Chung et al. (2005) estimate for 2001–2003 and the present study's for 2001–2004 are somewhat smaller than the 1999 INDOEX results at the surface, and the CCSM3 calculated forcing is even smaller. To gain insight into the differences in forcing estimates, we looked at the present study's aerosol forcing in each year. The surface forcing was $-12.8\,W/m^2$ in 2001, -14.7 in 2002, -10.9 in 2003 and -6.2 in 2004, giving a range of $-14.7 \sim -6.2\,W/m^2$. The

interannual fluctuation is very large and furthermore the INDOEX result is within our forcing estimates. Thus, it is concluded that the INDOEX results do not nullify the present study's estimate or Chung et al. (2005) but substantially undermine the credibility of the CCSM calculation.

Acknowledgements. The present study was initiated when Chung (first author) was at Scripps Institution of Oceanography, in response to a collaborative NASA project between Scripps Institution of Oceanography (SIO), Pacific Northwest National Laboratory (PNNL), and the University of Iowa. The authors are indebted to Drs. Kim and Feng of SIO for their help with literature search. This work was supported by a NASA grant (NNG04GC58G), USA. The Pacific Northwest National Laboratory is operated for the US Department of Energy by Battelle Memorial Institute under Contract DE-AC06-76RLO 1830. Additional funding in finishing the study came from the Academy of Finland Center of Excellence program (project number 1118615), Finland, and GIST Dasan start-up fund, Korea.

References

Ackerman, A. S., Toon, O. B., Stevens, D. E., Heymsfield, A. J., Ramanathan, V., and Welton, E. J.: Reduction of tropical cloudiness by soot, Science, 288, 1042–1047, 2000.

Adhikary, B., Carmichael, G. R., Tang, Y., Leung, L. R., Qian, Y., Schauer, J. J., Stone, E. A., Ramanthan, V., and Ramana, M. V.: Characterization of the seasonal cycle of South Asian aerosols: a regional-scale modeling analysis, J. Geophys. Res., 112, D22S22, doi:10.1029/2006JD008143, 2007.

Adhikary, B., Kulkarni, S., Dallura, A., Tang, Y., Chai, T., Leung, L. R., Qian, Y., Chung, C. E., Ramanathan, V., and Carmichael, G. R.: A regional scale chemical transport modeling of Asian aerosols with data assimilation of AOD observations using optimal interpolation technique, Atmos. Environ., 42(37), 8600–8615, 2008.

Albrecht, B. A.: Aerosols, cloud microphysics and fractional cloudiness, Science, 245, 1227–1230, 1989.

Carmichael, G. R., Tang, Y., Kurata, G., et al.: Evaluating regional emission estimates using the trace-p observations, J. Geophys. Res., 108(D21), 8810, doi:10.1029/2002JD003116, 2003.

Carmichael, G. R., Adhikary, B., Kulkarni, S., D'Allura, A., Tang, Y., Streets, D., Zhang, Q., Bond, T. C., Ramanathan, V., Jamroensan, A., and Marrapu, P.: Asian aerosols: current and year 2030 distributions and implications to human health and regional climate change, Environ. Sci. Technol., 43, 5811–5817, 2009.

Charlson, R. J., Langner, J., Rodhe, H., Leovy, C. B., and Warren, S. G.: Perturbation of the Northern Hemisphere radiative balance by black scattering from anthropogenic sulfate aerosols, Tellus A, 43, 152–163, 1991.

Chen, F. and Dudhia, J.: Coupling an advanced land surface – hydrology model with the Penn State – NCAR MM5 modeling system. Part I: model implementation and sensitivity, Mon. Weather Rev., 129, 569–585, 2001.

Chin, M., Ginoux, P., Kinne, S., Torres, O., Holben, B. N., Duncan, B. N., Martin, R. V., Logan, J. A., Higurashi, A., and Nakajima, T.: Tropospheric aerosol optical thickness from the GOCART model and comparisons with satellite and sunphotometer measurements, J. Atmos. Sci., 59, 461–483, 2002.

Chung, C. E., Ramanathan, V., Kim, D., and Podgorny, I. A.: Global anthropogenic aerosol direct forcing derived from satellite and ground-based observations, J. Geophys. Res., 110, doi:10.1029/2005JD006356, 2005.

Chung, C. E. and Zhang, G. J.: Impact of absorbing aerosol on precipitation: dynamic aspects in association with CAPE and convective parameterization closure, and dependence on aerosol heating profile. J. Geophys. Res., 109, D22103, doi:10.1029/2004JD004726, 2004.

Coakley, J. A. and Cess, R. D.: Response of the NCAR Community Climate Model to the radiative forcing by the naturally-occurring tropospheric aerosol, J. Atmos. Sci., 42, 1677–1692, 1985.

Collins, W. D., Rasch, P. J., Eaton, B. E., et al.: Simulating aerosols using a chemical transport model with assimilation of satellite aerosol retrievals: methodology for INDOEX, J. Geophys. Res., 106(D7), 7313–7336, 2001.

Collins, W. D., Blackmon, M. L., Bonanet, G. B., et al.: The Community Climate System Model Version 3 (CCSM3), J. Climate, 19(11), 2122-2143, doi:10.1175/JCLI3761.1, 2006.

Corrigan, C. E., Roberts, G. C., Ramana, M. V., Kim, D., and Ramanathan, V.: Capturing vertical profiles of aerosols and black carbon over the Indian Ocean using autonomous unmanned aerial vehicles, Atmos. Chem. Phys., 8, 737–747, 2008, http://www.atmos-chem-phys.net/8/737/2008/.

EANET: EANET Data on the Acid Deposition in the East Asian Region: 2004, from http://www.eanet.cc/product.html, 2004.
Giorgi, F., Bi, X., and Qian, Y.: Direct radiative forcing and regional climatic effects of anthropogenic aerosols over East Asia: a regional coupled climate-chemistry/aerosol model study, J. Geophys. Res., 107, 4439, doi:10.1029/2001JD001066, 2002.
Gong, S. L.: A parameterization of sea-salt aerosol source function for sub- and super-micron particles, Global Biogeochem. Cy., 17, 8/1–8/7, 2003.
Grell, G., Dudhia, J., and Stauffer, D. R.: A description of the fifth generation Penn State/NCAR mesoscale model (MM5). NCAR Tech. Note. NCAR/TN-3981IA, National Center for Atmospheric Research, Boulder, CO, 107 pp., 1995.
Gustafson, W. I. and Leung, L. R.: Regional downscaling for air quality assessment: a reasonable proposition? B. Am. Meteorol. Soc., 88(8), 1215–1227, 2007.
Guttikunda, S. K., Tang, Y., Carmichael, G. R., et al.: Impacts of Asian megacity emissions on regional air quality during spring 2001, J. Geophys. Res., 110, D20301, doi:10.1029/2004JD004921, 2005.
Hong, S.-Y. and Pan, H.-L.: Nonlocal boundary layer vertical diffusion in a medium-range forecast model, Mon. Weather Rev., 124, 2322–2339, 1996.
Huebert, B. J., Bates, T., Russell, P. B., Shi, G., Kim, Y. J., Kawamura, K., Carmichael, G. R., and Nakajima, T.: An overview of ACE-Asia: strategies for quantifying the relationships between asian aerosols and their climatic impacts, J. Geophys. Res., ACE-Asia Special Issue A 8633, 108(D23), 8633, doi:10.1029/2003JD003550, 2003.
Kain, J. S. and Fritsch, J. M.: Convective parameterization in mesoscale models: the Kain-Fritsch scheme. The Representation of Cumulus Convection in Numerical Models, Meteor. Monogr., No. 24, Amer. Meteor. Soc., 165–170, 1993.
Khattatov, B. V., Lamarque, J.-F., Lyjak, L. V., et al.: Assimilation of satellite observations of long-lived chemical species in global chemistry transport models, J. Geophys. Res., 105, 29135–29144, 2000.
Kiehl, J. T., Hack, J. J., and Briegleb, B. P.: The simulated earth radiation budget of the National Center for Atmospheric Research Community Climate Model CCM2 and comparisons with the Earth Radiation Budget Experiment, J. Geophys. Res., 99, 20815–20827, 1994.
Kim, D. and Ramanathan, V.: Solar radiation budget and radiative forcing due to aerosols and clouds, J. Geophys. Res., 113, D02203, doi:10.1029/2007JD008434, 2008.

Kinne, S., Lohmann, U. Feichter, J., et al.: Monthly averages of aerosol properties: A global comparison among models, satellite data, and AERONET ground data, J. Geophys. Res., 108, 4634, doi:10.1029/2001JD001253, 2003.

Kistler, R., Kalnay E., Collins, W., et al.: The NCEP-NCAR 50-year reanalysis: Monthly means CD-ROM and documentation, B. Am. Meteorol. Soc., 82(2), 247–267, 2001.

Koch, D., Schulz, M., Kinne, S., McNaughton, C., Spackman, J. R., Balkanski, Y., Bauer, S., Berntsen, T., Bond, T. C., Boucher, O., Chin, M., Clarke, A., De Luca, N., Dentener, F., Diehl, T., Dubovik, O., Easter, R., Fahey, D. W., Feichter, J., Fillmore, D., Freitag, S., Ghan, S., Ginoux, P., Gong, S., Horowitz, L., Iversen, T., Kirkevåg, A., Klimont, Z., Kondo, Y., Krol, M., Liu, X., Miller, R., Montanaro, V., Moteki, N., Myhre, G., Penner, J. E., Perlwitz, J., Pitari, G., Reddy, S., Sahu, L., Sakamoto, H., Schuster, G., Schwarz, J. P., Seland, Ø., Stier, P., Takegawa, N., Takemura, T., Textor, C., van Aardenne, J. A., and Zhao, Y.: Evaluation of black carbon estimations in global aerosol models, Atmos. Chem. Phys., 9, 9001–9026, 2009, http://www.atmos-chem-phys.net/9/9001/2009/.

Leung, L. R., Zhong, S., Qian, Y., and Liu, Y.: Evaluation of regional climate simulations of the 1998 and 1999 East Asian summer monsoon using the GAME/HUBEX observational data, J. Meteorol. Soc. Japan, 82(6), 1695–1713, 2004.

Leung, L. R., Qian, Y. and Bian, X.: Hydroclimate of the western United States based on observations and regional climate simulation of 1981–2000. Part I: seasonal statistics, J. Climate, 16, 1892–1911, 2003.

Lorenc, A. C.: Analysis methods for numerical weather prediction, Q. J. Roy. Meteor. Soc., 112, 1177–1194, 1986.

Myhre, G.: Consistency between satellite-derived and modeled estimates of the direct aerosol effect, Science, 325(5937), 187–190, doi:10.1126/science.1174461, 2009.

Olivier, J. G. J. and Berdowski, J. J. M.: Global emissions sources and sinks, A. A. Balkema Publishers/Swets and Zeitlinger Publishers, The Netherlands, 33–78, 2001.

Penner, J. E., Andreae, M., Annegarn, H., Barrie, L., Feichter, J., Hegg, D., Jayaraman, A., Leaitch, R., Murphy, D., Nganga, J., and Pitari, G.: Aerosols, their direct and indirect effects, IPCC 3rd Assessment Report, Chap. 5, 2001.

Podgorny, I. A., Conant, W. C., Ramanathan, V., and Satheesh, S. K.: Aerosol modulation of atmospheric and solar heating over the tropical Indian Ocean, Tellus B, 52, 947–958, 2000.

Podgorny, I. A. and Ramanathan, V.: A modeling study of the direct effect of aerosols over the Tropical Indian Ocean, J. Geophys. Res., 106, 24097–24105, 2001.

Ramana, M. V., Ramanathan, V., Kim, D., Roberts, G. C., and Corrigan, C. E.: Albedo, atmospheric solar absorption and heating rate measurements with stacked UAVs, Q. J. Roy. Meteor. Soc., 133, 1913–1931, 2007.

Ramanathan, V., Crutzen, P. J., Lelieveld, J., et al.: The Indian Ocean experiment: an integrated analysis of the climate forcing and effects of the great Indo-Asian haze, J. Geophys. Res, 106, 28371–28398, 2001.

Ramanathan, V., Ramana, M. V., Roberts, G., Kim, D., Corrigan, C., Chung C., and Winker, D.: Warming trends in Asia amplified by brown cloud solar absorption, Nature, 448, 575–578, doi:10.1038/nature06019, 2007.

Ramanathan, V. and Carmichael, G.: Global and regional climate changes due to black carbon, Nat. Geosci., 1, 221–227, 2008.

Reisner, J., Rasmussen, R. J., and Bruintjes, R. T.: Explicit forecasting of supercooled liquid water in winter storms using the MM5 mesoscale model, Q. J. Roy. Meteor. Soc., 124B, 1071–1107, 1998.

Rosenfeld, D.: Suppression of rain and snow by urban and industrial air pollution, Science, 287, 1793–1796, 2000.

Rossow, W. B. and Schiffer, R. A.: Advances in understanding clouds from ISCCP, B. Am. Meteorol. Soc., 80, 2261–2287, 1999.

Qian, Y. and Leung, L. R.: A long-term regional simulation and observations of the hydroclimate in China, J. Geophys. Res., 112, D14104, doi:10.1029/2006JD008134, 2007.

Satheesh, S. K., Ramanathan, V., Xu, L.-J., Lobert, J. M., Podgorny, I. A., Prospero, J. M., Holben, B. N., and Loeb, N. G.: A model for the natural and antropogenic aerosols over the tropical Indian Ocean derived from Indian Ocean experiment data, J. Geophys. Res., 104, 27421–27440, 1999.

Streets, D. G., Bond, T. C., Carmichael, G. R., et al.: An inventory of gaseous and primary aerosol emissions in Asia in the year 2000, J. Geophys. Res., 108, GTE 30/31–GTE 30/23, 2003.

Tang, Y., Carmichael, G. R., Kurata, G., et al.: Impacts of dust on regional tropospheric chemistry during the ACE-Asia experiment: a model study with observations, J. Geophys. Res., 109, D19S21, doi:10.1029/2003JD003806. 2003.

Textor, C., Schulz, M., Guibert, S., Kinne, S., Balkanski, Y., Bauer, S., Berntsen, T., Berglen, T., Boucher, O., Chin, M., Dentener, F., Diehl, T., Easter, R., Feichter, H., Fillmore, D., Ghan, S., Ginoux, P., Gong, S., Grini, A., Hendricks, J., Horowitz, L., Huang, P., Isaksen, I., Iversen,

I., Kloster, S., Koch, D., Kirkevåg, A., Kristjansson, J. E., Krol, M., Lauer, A., Lamarque, J. F., Liu, X., Montanaro, V., Myhre, G., Penner, J., Pitari, G., Reddy, S., Seland, Ø., Stier, P., Takemura, T., and Tie, X.: Analysis and quantification of the diversities of aerosol life cycles within AeroCom, Atmos. Chem. Phys., 6, 1777–1813, 2006, http://www.atmos-chem-phys.net/6/1777/2006/.

Twomey, S.: Atmospheric Aerosols, Elsevier Sci., New York, 302 pp., 1997.

van der Werf, G. R., Randerson, J. T., Giglio, L., Collatz, G. J., Kasibhatla P. S., and Arellano Jr., A. F.: Interannual variability in global biomass burning emissions from 1997 to 2004, Atmos. Chem. Phys., 6, 3423–3441, 2006, http://www.atmos-chem-phys.net/6/3423/2006/.

Xie, P. and Arkin, P. A.: Analyses of global monthly precipitation using gauge observations, satellite estimates, and numerical model predictions, J. Climate, 9, 840–858, 1996.

Yu, H., Kaufman, Y. J., Chin, M., Feingold, G., Remer, L. A., Anderson, T. L., Balkanski, Y., Bellouin, N., Boucher, O., Christopher, S., DeCola, P., Kahn, R., Koch, D., Loeb, N., Reddy, M. S., Schulz, M., Takemura, T., and Zhou, M.: A review of measurement-based assessments of the aerosol direct radiative effect and forcing, Atmos. Chem. Phys., 6, 613–666, 2006, http://www.atmos-chem-phys.net/6/613/2006/.

Zhang, Q., Streets, D. G., Carmichael, G. R., He, K. B., Huo, H., Kannari, A., Klimont, Z., Park, I. S., Reddy, S., Fu, J. S., Chen, D., Duan, L., Lei, Y., Wang, L. T., and Yao, Z. L.: Asian emissions in 2006 for the NASA INTEX-B mission, Atmos. Chem. Phys., 9, 5131–5153, 2009, http://www.atmos-chem-phys.net/9/5131/2009/.

Table 1. Aerosol radiative forcing averaged in Asia (60–138° E and Eq. −45° N). This table compares the present study's calculations with those derived from Chung et al. (2005). Both studies used the MODIS and AERONET aerosol observations while the primary differences are i) aerosol vertical profile simulated by a high-resolution model in this study (as opposed to a prescribed uniform aerosol profile in Chung et al., 2005) and ii) different aerosol-chemistry models used to fill up aerosol data gaps.

	Present study (anthropogenic aerosol)	Present study (BC aerosol)	Chung et al. (2005) (anthropogenic aerosol)	Chung et al. (2005) (BC aerosol)
Toa	$-1.3\,W/m^2$	+2.1	−1.1	+2.3
Atmosphere	+7.3	+7.3	+8.0	+7.6
Surface	−8.6	−5.2	−9.1	−5.3

Table 2. Anthropogenic aerosol radiative forcing averaged over the INDOEX domain (40–100° E and Eq. −20° N) for the January–March period. The forcing estimate for the year 1999 from the INDOEX (Indian Ocean experiment) is shown along with Chung et al. (2005) estimate for 2001–2003, the present study's estimate for 2001–2004 and the CCSM calculation. For the present study's estimate, we also show the range from an estimate for each year.

	INDOEX results (Ramanathan et al., 2001)	Chung et al. (2005)	Present study	NCAR/CCSM3
TOA	−2.5~+0.5 W/m^2	−2.9	−3.6 (−1.9~−4.5)	−1.1
Atmosphere		+7.6	+7.6 (+4.3~+10.4)	+4.5
Surface	−18~−14	−10.5	−11.1 (−14.7~−6.2)	−5.6

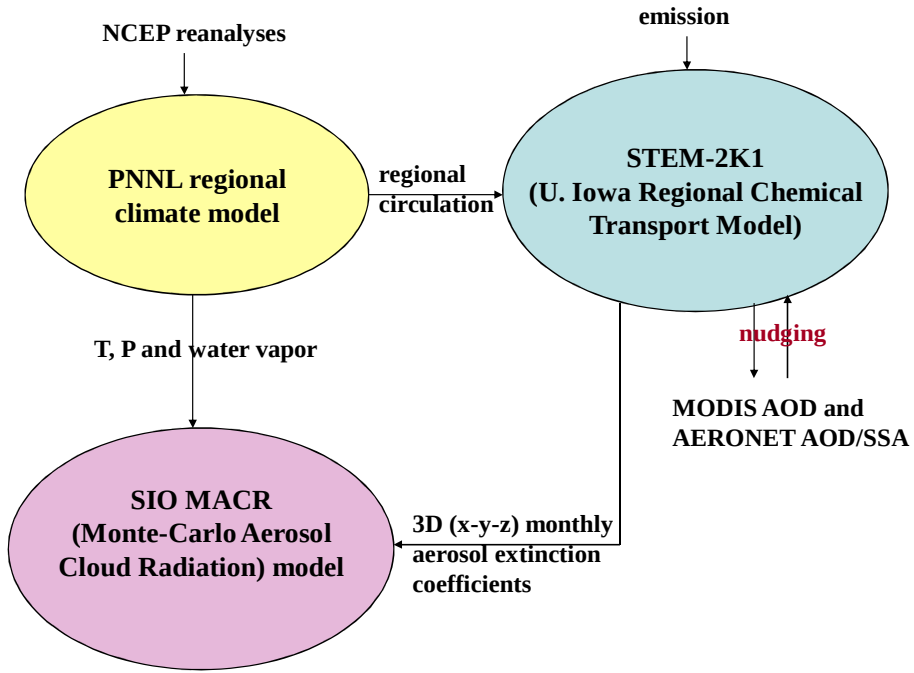

Fig. 1. Overview of the Asian aerosol assimilation project. The project has been a joint effort between Scripps Institution of Oceanography (SIO), Pacific Northwest National Laboratory (PNNL) and the University of Iowa. The SIO MACR (Monte-Carlo Aerosol Cloud Radiation) model took aerosol simulations from Iowa STEM (Sulfur Transport dEposition Model), meteorological variables from the PNNL regional model, and cloud from the ISCCP, so as to produce 2001–2004 aerosol radiative forcing.

ACPD
10, 821–862, 2010

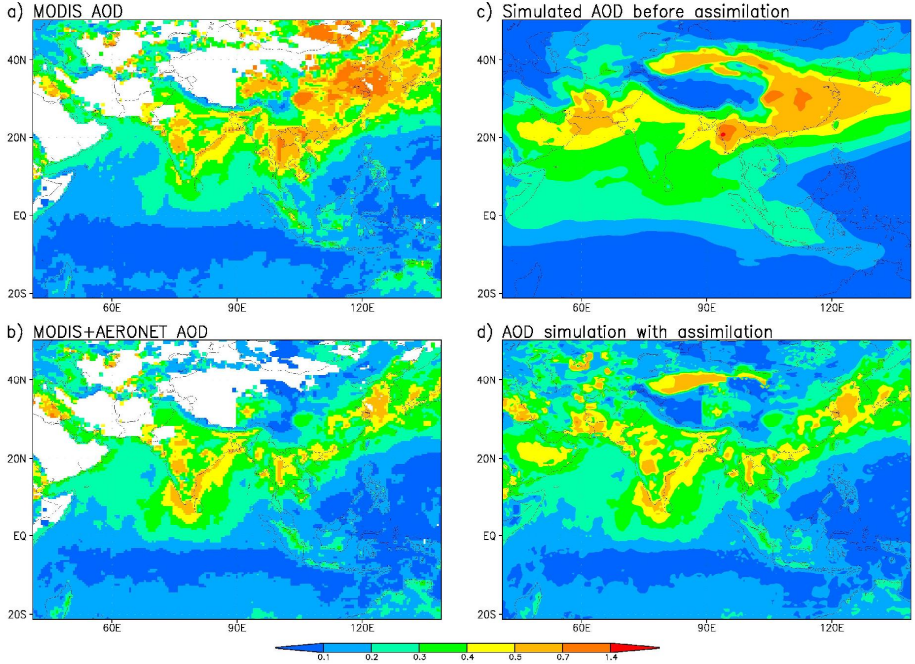

Fig. 2. Total (natural+anthropogenic) AOD (Aerosol Optical Depth). **(a)** Monthly AOD observation in March, 2001, from the satellite MODIS instrument. **(b)** March 2001 AOD adjusted with scattered ground observations AERONET. **(c)** Simulated AODs by the STEM-2K1 model (March 2001). **(d)** AOD simulation after assimilating MODIS+AERONET AOD.

ACPD
10, 821–862, 2010

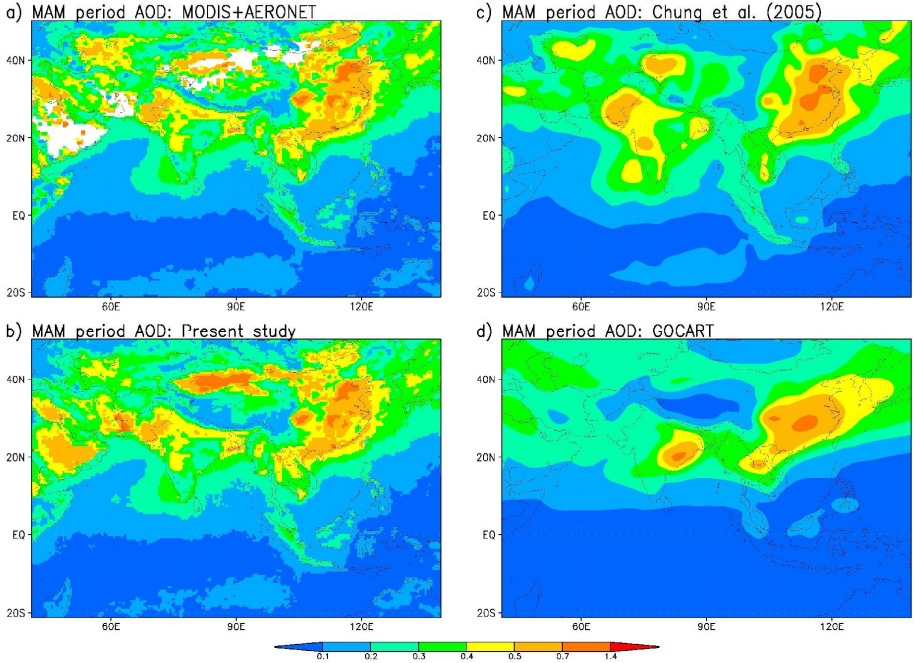

Fig. 3. Total (natural+anthropogenic) AOD simulation in comparison with that in Chung et al. (2005) and the GOCART AOD simulation. AERONET/MODIS integrated AODs are also shown **(a)**. Note that our simulation is 2001–2004 mean while Chung et al. (2005) calculation was for 2001–2003 and the GOCART simulation is averaged from 2000 to 2002.

ACPD
10, 821–862, 2010

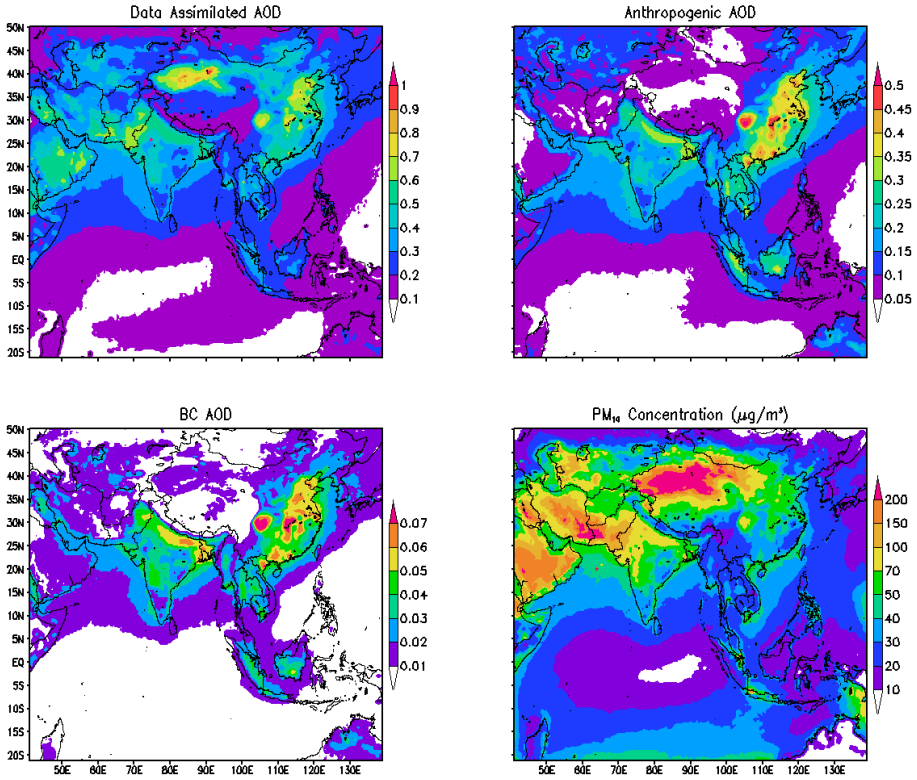

Fig. 4. Four-year mean model fields after assimilation of AOD, anthropogenic AOD, BC AOD and surface PM_{10} mass concentration ($\mu g/m^3$).

ACPD
10, 821–862, 2010

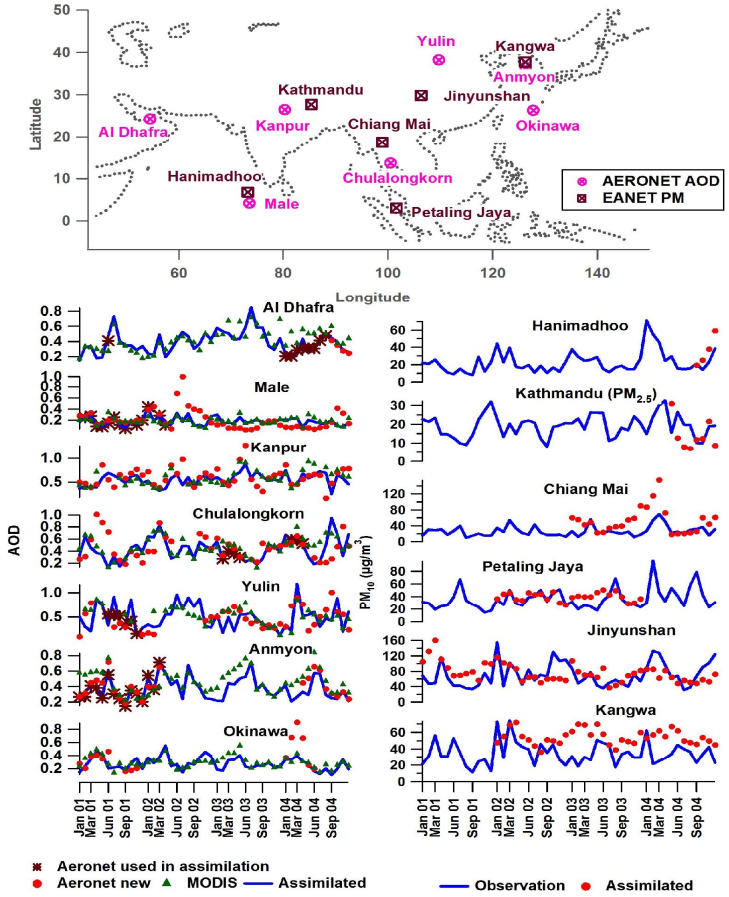

Fig. 5. AOD (left panels) and surface PM_{10} mass concentration (right panels). Modeled AOD and PM_{10} concentration after assimilation, in comparison with MODIS and AERONET AODs and EANET PM_{10} observations at selected sites. The AERONET AODs used in the assimilation are also shown.

ACPD
10, 821–862, 2010

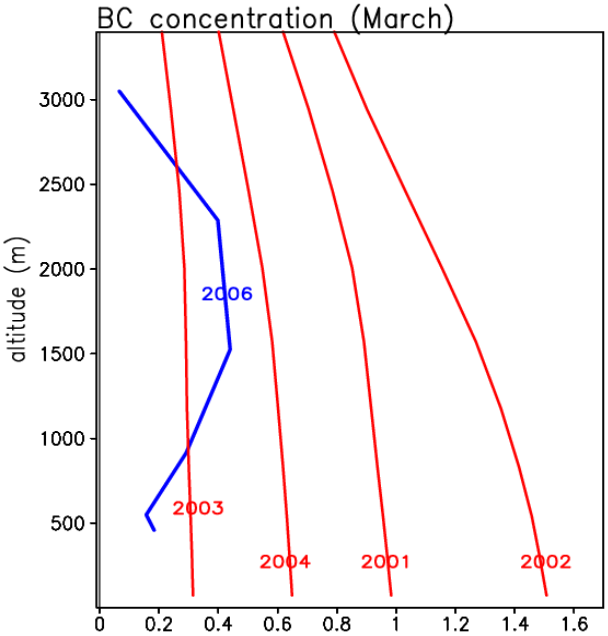

Fig. 6. Monthly BC (black carbon) concentration comparison (in units of μg/m^3). Blue line displays the MAC observation data over 73.18° E and 6.78° N during March 2006 (Ramanathan et al., 2007). Red lines show the present model calculation at a nearby grid (73.36° E and 6.6° N) in March 2001, 2002, 2003 and 2004, respectively.

ACPD
10, 821–862, 2010

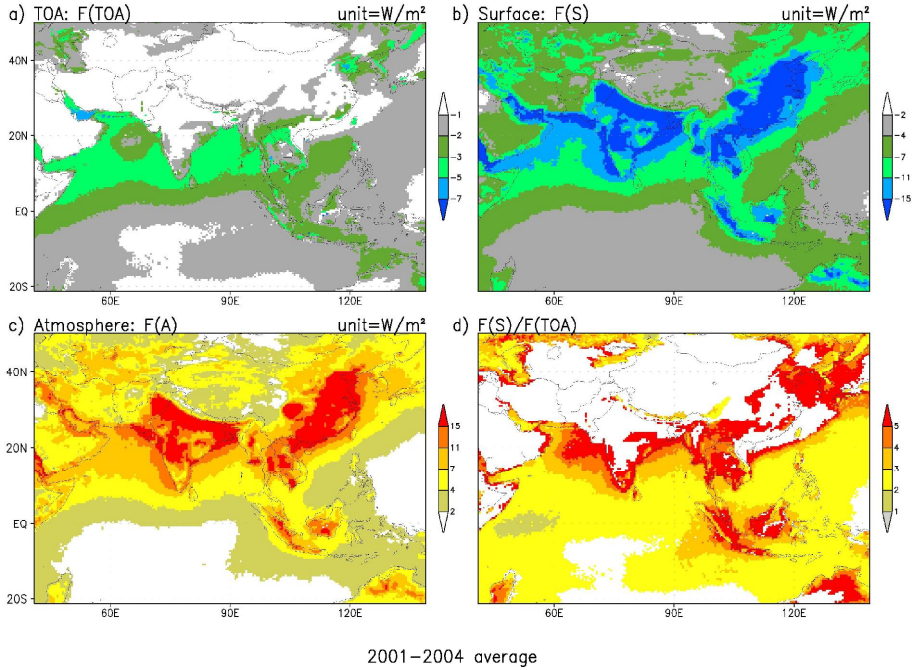

Fig. 7. Anthropogenic direct aerosol radiative forcing averaged over the entire 2001–2004 period. In this and subsequent figures, the forcing estimates are for cloudy skies.

ACPD
10, 821–862, 2010

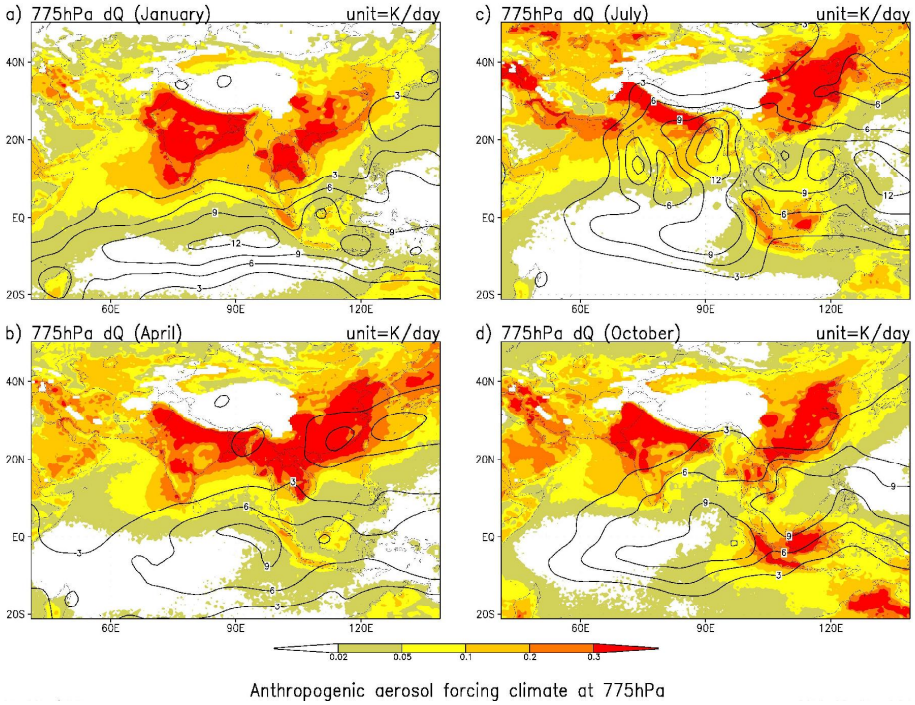

Fig. 8. Monthly anthropogenic aerosol radiative forcing averaged from 2001 to 2004. Contours are observed climatological precipitation in units of mm/day. Note that the PNNL model precipitation simulation in this study is similar to the observation in pattern.

ACPD
10, 821–862, 2010

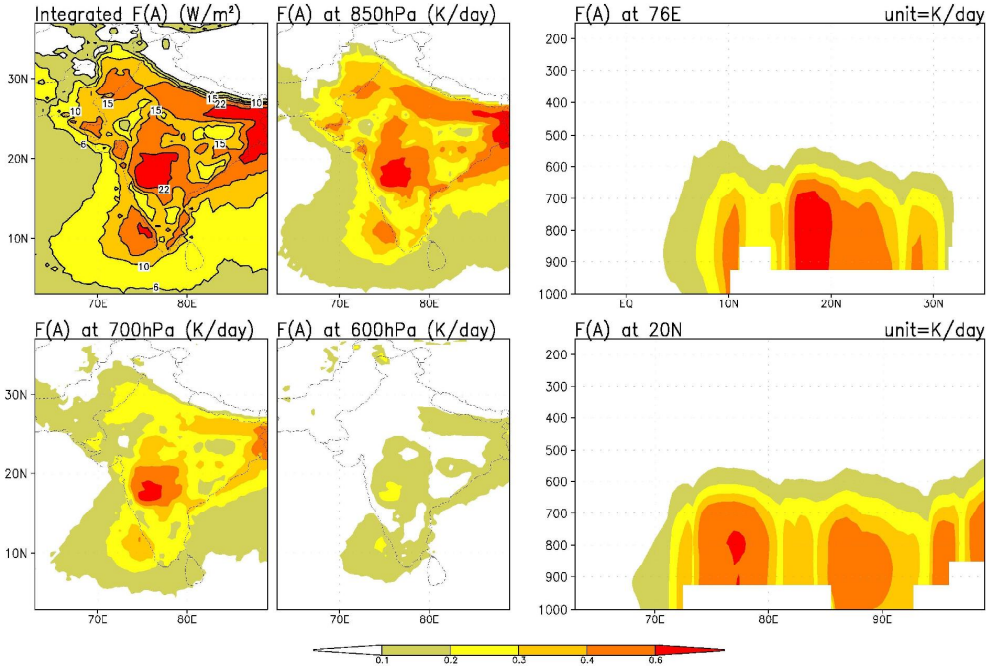

Fig. 9. Anthropogenic aerosol forcing in the atmosphere for February (averaged from 2001 to 2004).

ACPD
10, 821–862, 2010

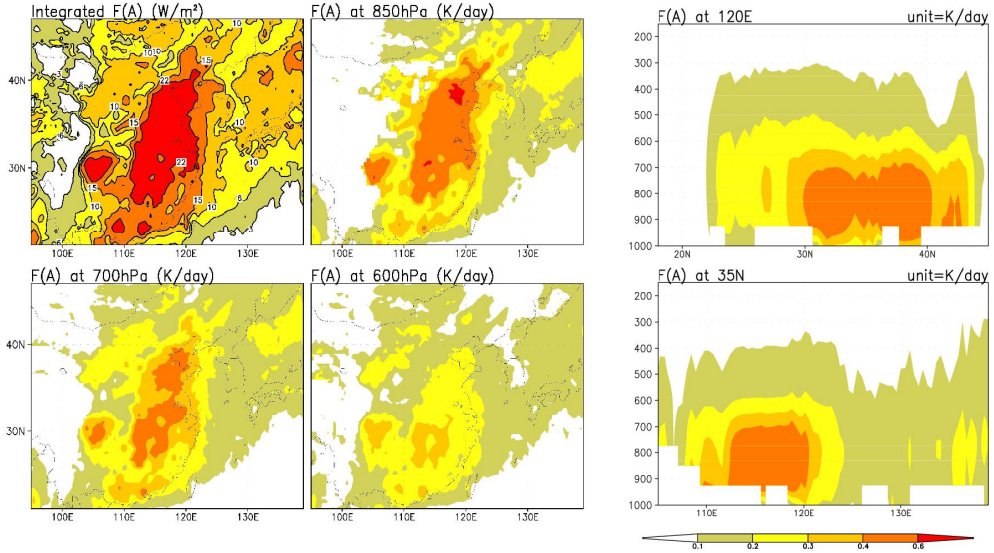

Fig. 10. Anthropogenic aerosol forcing in the atmosphere for May (averaged from 2001 to 2004).

ACPD
10, 821–862, 2010

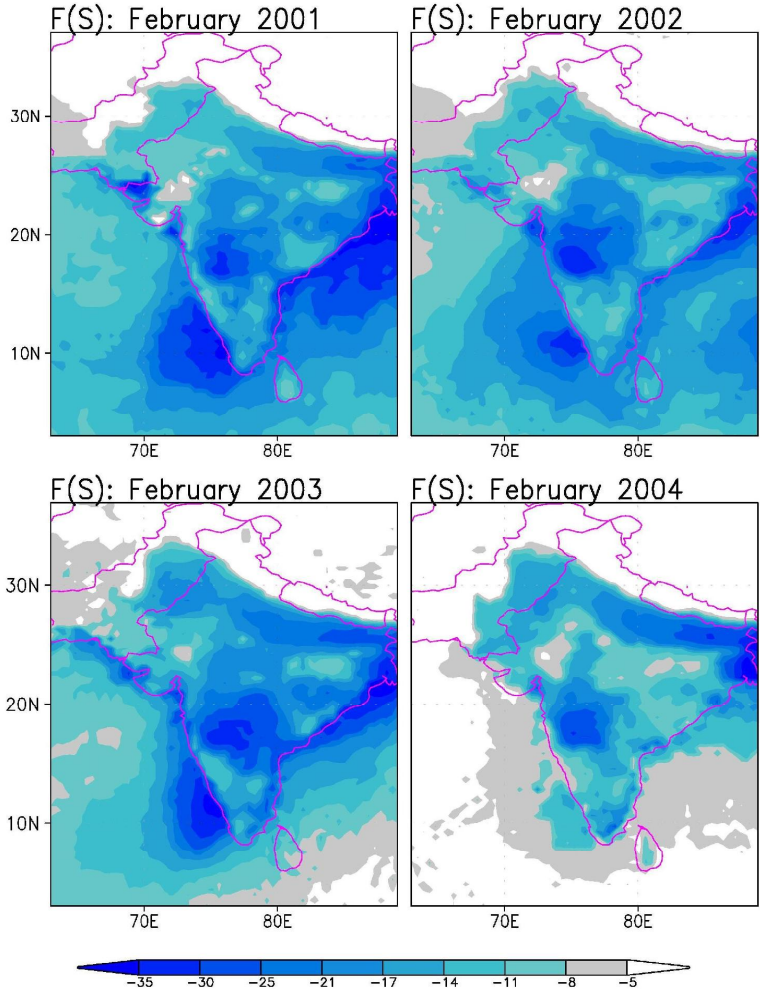

Fig. 11. Anthropogenic aerosol forcing at the surface in units of W m^{-2}.

ACPD
10, 821–862, 2010

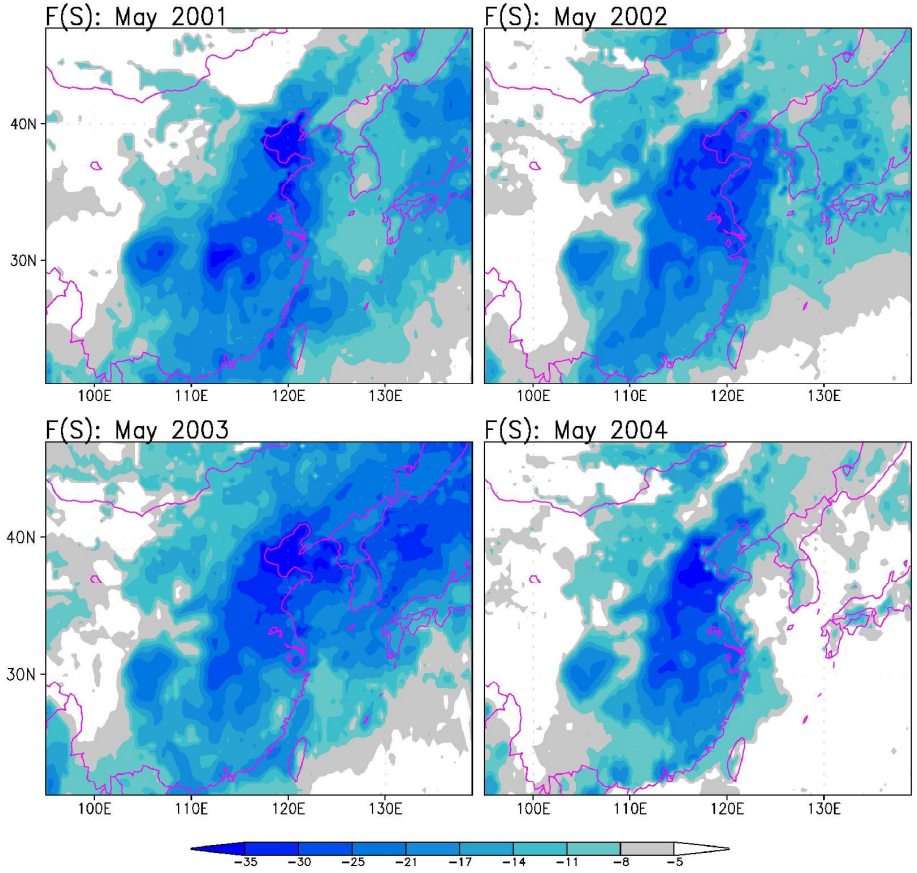

Fig. 12. Anthropogenic aerosol forcing at the surface in units of W m^{-2}.

ACPD
10, 821–862, 2010

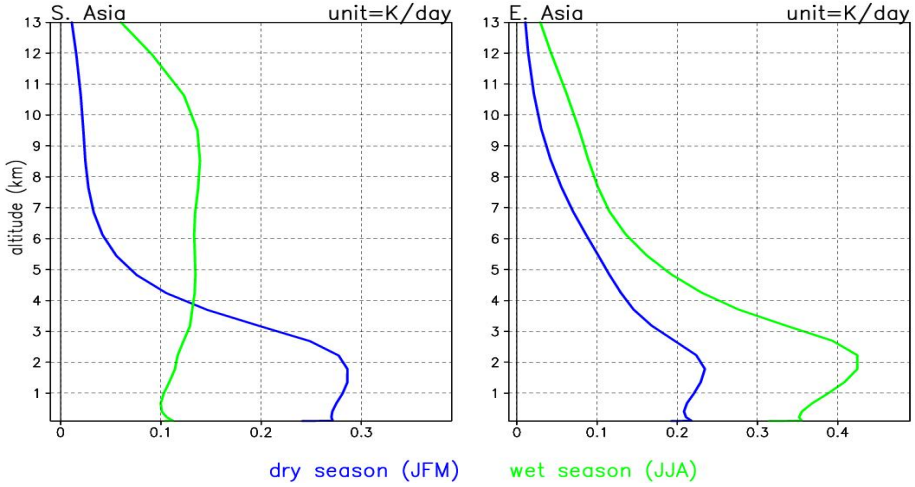

Fig. 13. Vertical profile of climatological anthropogenic aerosol forcing in units of K/day. Plotted are area averages for South Asia (70–90° E and 5–25° N) and East Asia (115–125° E and 30–40° N).

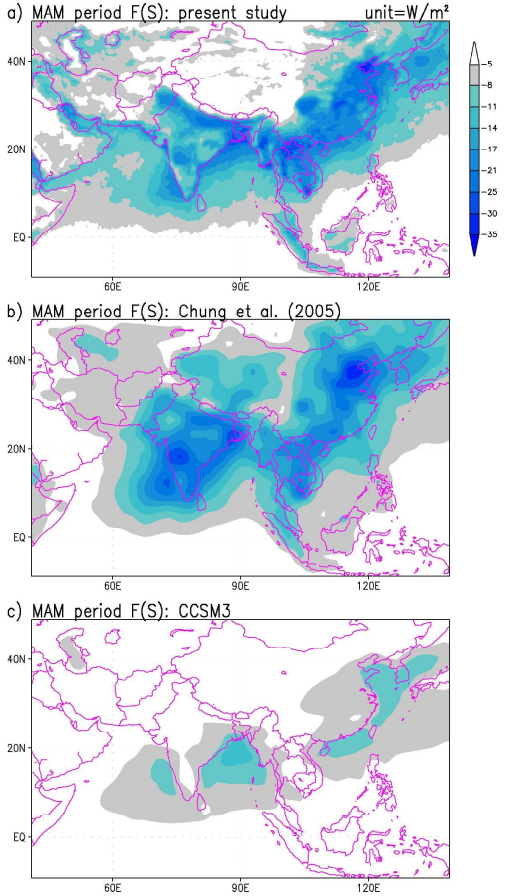

Fig. 14. Comparison of anthropogenic aerosol forcing at the surface: F(S), in units of $W\,m^{-2}$. **(a)** F(S) averaged from March to May and from 2001 to 2004 in this study. **(b)** MAM (March, April, May) period F(S) from Chung et al. (2005) estimate. **(c)** MAM period F(S) from the NCAR CCSM3.0. Shown in all the panels are average-sky aerosol forcing estimates.

ACPD
10, 821–862, 2010